



Processes affecting solute transport through soils : preferential flow and microbial degradation
by Heiko Walter Langner

A thesis submitted in partial fulfillment of the requirements for the degree of Doctor of Philosophy in
Crop and Soil Science

Montana State University

© Copyright by Heiko Walter Langner (1997)

Abstract:

Preferential flow of water through soil macropores has been of concern because it may be a source of accelerated contaminant transport into underlying groundwater. We designed an experimental system to study effects of soil matric potential (h) on the occurrence of nonequilibrium (preferential) flow conditions in four intact cores (15 cm diameter, 30 cm length) of a permanent grassland soil. Nonequilibrium transport of a nonsorbing tracer ($^3\text{H}_2\text{O}$) was consistently observed at $h > -5$ cm, while equilibrium conditions were consistent at $h < -10$ cm. This suggests that soil pores with equivalent radii larger than 150 to 300 μm may contribute to preferential flow. However, no relationship between the soil volume occupied by macropores and preferential flow was identified. Although the onset of nonequilibrium transport was associated with increases in pore water velocity (v) within each individual soil column, no consistent dependency of the occurrence of nonequilibrium on v was observed among replicate soil columns. Since the pore water velocities associated with preferential flow observed in the current study are often exceeded under local climatic conditions, preferential flow events may be important under local field conditions.

For many organic solutes, microbial degradation is one of the most important processes controlling contaminant fate and transport. We used 2,4-dichlorophenoxyacetic acid (2,4-D) as a model compound to (i) test the applicability of first-order and logistic growth models for describing microbial degradation under batch and transport conditions, (ii) determine the applicability of batch-derived degradation parameters under a wide range of transport conditions, and (iii) separate effects of column residence time (RT) and v on degradation rate parameters. Degradation of 2,4-D under batch conditions was best described by a logistic growth model. Under transport conditions (repacked soil columns), a continuous pulse of 1 mg L⁻¹ 2,4-D in the eluent solution resulted in a wide range of steady state 2,4-D effluent concentrations (0.063-0.92 mg L⁻¹). Although degradation of 2,4-D under transport conditions was best described by first-order degradation kinetics, estimated first-order degradation rate constants (μs) ranged from 0.007 to 0.071 h⁻¹ as a function of v . Estimated values of μs were not correlated with RT, but could be explained by invoking a relationship between v and a local opportunity time (time per unit length).

PROCESSES AFFECTING SOLUTE TRANSPORT THROUGH SOILS:
PREFERENTIAL FLOW AND MICROBIAL DEGRADATION

by

Heiko Walter Langner

A thesis submitted in partial fulfillment
of the requirements for the degree

of

Doctor of Philosophy

in

Crop and Soil Science

MONTANA STATE UNIVERSITY-BOZEMAN
Bozeman, Montana

April 1997

D378
22672


APPROVAL

of a thesis submitted by

Heiko Walter Langner

This thesis has been read by each member of the thesis committee and has been found to be satisfactory regarding content, English usage, format, citations, bibliographic style, and consistency, and is ready for submission to the College of Graduate Studies.

William P. Inskeep
(Graduate Committee, Chair)

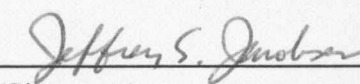


(Signature)

4/18/97
(Date)

Approved for the Department of Plant, Soil & Environmental Sciences

Jeffrey S. Jacobsen
(Department Head)

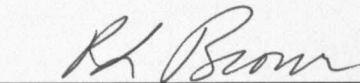


(Signature)

4/18/97
(Date)

Approved for the College of Graduate Studies

Robert L. Brown
(Graduate Dean)



(Signature)

4/22/97
(Date)

STATEMENT OF PERMISSION TO USE

In presenting this thesis in partial fulfillment of the requirements for a doctoral degree at Montana State University-Bozeman, I agree that the Library shall make it available to borrowers under rules of the Library. I further agree that copying of this thesis is allowable only for scholarly purposes, consistent with "fair use" as prescribed in the U.S. Copyright Law. Requests for extensive copying or reproduction of this thesis should be referred to University Microfilms International, 300 North Zeeb Road, Ann Arbor, Michigan 48106, to whom I have granted "the exclusive right to reproduce and distribute my dissertation in and from microform along with the non-exclusive right to reproduce and distribute my abstract in any format in whole or in part."

Signature _____

Heiko Cangel

Date _____

4 / 18 / 97

ACKNOWLEDGEMENTS

I would like to thank my major advisor Dr. William Inskeep for the ideas, support and encouragement he has given me as a graduate student at Montana State University–Bozeman.

I would also like to thank the other members of my graduate committee, Dr. Jon Wraith, Dr. Warren Jones, Dr. James Bauder, and Dr. Stephan Custer for their assistance.

My special thanks go to my fellow lab workers Dr. Hesham Gaber, Clain Jones, Jeffrey Darland, Richard Macur, Dr. Robert Grosser, Dr. Shaobai Sun, and Dr. Bhabani Das. I thank Sarah Olson and the other students who helped me with the laboratory work.

I owe thanks to the German foundation Studienstiftung des Deutschen Volkes for funding part of my research, and Prof. Bernd Huwe for his altruistic help in securing this funding.

I am especially grateful to Prof. Horst Mutscher who introduced me to the world of soils. I am indebted to Dr. Earl Skogley and Dr. Achim Dobermann for encouraging me to live and study in this beautiful area.

Finally, I would like to give special thanks to my family, Ute and Adelheid, and to our parents for their loving support.

TABLE OF CONTENTS

APPROVAL	ii
STATEMENT OF PERMISSION TO USE	iii
VITA	iv
ACKNOWLEDGEMENTS	v
TABLE OF CONTENTS	vi
LIST OF TABLES	viii
LIST OF FIGURES	ix
ABSTRACT	xii
1. INTRODUCTION	1
2. APPARATUS FOR CONSTANT-POTENTIAL SOLUTE TRANSPORT AND SOIL WATER CHARACTERISTIC DETERMINATION	6
INTRODUCTION	6
MATERIALS AND METHODS	8
Measurement of Soil Water Characteristic	12
Setting Unit Potential Gradient	13
Monitoring Column Hydraulic Conditions	14
3. PREFERENTIAL FLOW THROUGH INTACT SOIL CORES: EFFECTS OF MATRIC POTENTIAL	17
INTRODUCTION	17
MATERIALS AND METHODS	20
Soil	20
Experimental Setup	20
Transport Experiments	21
Modeling	22
Local Equilibrium Assumption	23

Physical Nonequilibrium	24
Estimating Transport Parameters from Breakthrough Curves	27
Criteria for Distinguishing Equilibrium vs Nonequilibrium Transport	28
Soil Water Characteristic and Pore Size Distribution	29
RESULTS AND DISCUSSION	30
Effects of Matric Potential	30
Effects of Soil Properties	34
Pore Water Velocity and Matric Potential	41
Pore Water Velocity and Physical Nonequilibrium	42
4. PORE WATER VELOCITY AND RESIDENCE TIME EFFECTS ON THE DEGRADATION OF 2,4-D DURING TRANSPORT	46
INTRODUCTION	46
MATERIALS AND METHODS	49
Soil	49
Batch Sorption Isotherms	49
Batch Degradation Experiments	51
Column Transport Experiments	52
Modeling Approaches	55
Batch Degradation Models	56
Logistic Growth Model	56
First-Order Degradation Model	58
Transport Experiments	59
Dispersion Coefficients and Retardation Factors	59
Transport Model Predictions	60
RESULTS AND DISCUSSION	61
Batch Sorption Isotherms	61
2,4-D Degradation under Batch Conditions	62
Transport Experiments	65
Behavior of $^3\text{H}_2\text{O}$	65
Sterile Control Column Experiment	67
2,4-D Transport under Nonsterile Conditions	69
Transport Simulations with Logistic Growth Model	72
Transport Modeling with First-Order Degradation	75
Effects of Pore Water Velocity on 2,4-D Degradation Rate Constants ..	77
5. SUMMARY	82
REFERENCES CITED	88

LIST OF TABLES

Table

1. Experimental conditions of the transport experiments using four undisturbed soil cores, and optimized model parameters from fitting $^3\text{H}_2\text{O}$ BTCs to solute transport models based on local equilibrium (LEA) and physical nonequilibrium (PNE) models	32
2. Optimized parameters from fitting van Genuchten's (1980) model to $\theta(h)$ data collected during wetting and drying cycles of selected soil columns	38
3. Experimental conditions for the column experiments	52
4. Estimated parameters obtained by fitting the logistic growth model to CO_2 evolution data of 2,4-D degradation experiments conducted under various batch conditions	64
5. Resulting parameters from fitting the physical NE model to the $^3\text{H}_2\text{O}$ BTCs	65
6. The fate of 2,4-D in soil column experiments	71
7. Estimated first-order degradation rate constants and nonequilibrium parameters for nonsterile column experiments obtained using different modeling approaches (values of R_f and D obtained independently)	76

LIST OF FIGURES

Figure

1. Schematic diagram of soil column control and monitoring system with valves in collecting mode (a) and sampling mode (b). 9
2. Experimental wetting and drying curves for one TDR waveguide-tensiometer pair. The wetting and drying limbs were individually fit to the van Genuchten (1980) model 12
3. Measured soil water content (θ) during a $^3\text{H}_2\text{O}$ miscible displacement experiment at $h = -24$ cm. Upper and lower θ refer to two TDR probe positions in the intact soil column. Increasing θ indicates gradually degrading pore system in the upper layer of the core after two previous leaching experiments (approximately 10 pore volumes) with insignificant changes 15
4. Measured soil water content (a) and soil matric potential (b) during a $^3\text{H}_2\text{O}$ miscible displacement experiment at $h = -5$ cm. Upper and lower θ or h refer to two TDR probe or tensiometer positions in the intact soil column. The irregularity in h at about 0.7 pore volumes indicates slight flow disruption during switching of eluent from pulse to background solution 16
5. Example series of observed and fitted (LEA and PNE models) BTCs collected with soil column PN11 at various values of h . Each plot contains two series of soil matric potentials measured at the two tensiometer locations. Note the positive pressures at both tensiometer positions in D, which were caused by low hydraulic conductivity of the bottom porous plate 31
6. Water characteristic relationships [$\theta(h)$] for soil column PN14 generated at two depths (8 and 20 cm). Symbols represent measured $\theta(h)$ values, lines are least square fits to the van Genuchten (1980) model (optimized parameter values are shown in Table 2) 35
7. Fitted wetting (A) and drying curves (B) for both upper (closed symbols) and lower (open symbols) instrumented positions (indicated in legend by U or L, respectively). Optimized parameters (Table 2) were obtained by fitting van Genuchten's (1980, Eq. [16]) model to $\theta(h)$ pairs between $h = 0$ and -70 cm 37

8. Estimated drained porosities [$\theta_s - \theta(h)$] derived from the $\theta(h)$ curves shown in Fig. 7. Minimum drained pore radii (r) were calculated as a function of h using Eq. [17]	39
9. Example series of observed and fitted (LEA and PNE models) BTCs at various values of h collected for experiments having similar v	44
10. Diagram of the experimental apparatus for solute transport and degradation studies in soil columns	53
11. Degradation of ^{14}C -2,4-D (measured as fraction of total added ^{14}C recovered as $^{14}\text{CO}_2$, P/S_0) in batch experiments performed under various conditions. Error bars for moist, previously dry soil were generated using data from all soil water contents tested. Filled symbols represent initial aqueous phase 2,4-D concentrations of 1.0 mg L^{-1} ; open symbols represent 0.1 mg L^{-1} initial aqueous phase 2,4-D concentration	62
12. $^3\text{H}_2\text{O}$ breakthrough curves of all column experiments. Identical symbol fills represent identical column lengths; identical symbol shapes designate identical target residence times	66
13. Observed and predicted [LEA model using independent estimates of R_f (3.89) and D ($0.22 \text{ cm}^2 \text{ h}^{-1}$)] 2,4-D breakthrough curves (BTCs) for sterile column experiment. Fitted BTCs were generated using (i) the LEA model where R_f was optimized (3.49) and (ii) the chemical nonequilibrium model where nonequilibrium parameters were optimized ($\beta = 0.76$, $\omega = 0.42$) using fixed R_f (3.89) and D ($0.22 \text{ cm}^2 \text{ h}^{-1}$)	68
14. Comparison of observed and predicted 2,4-D BTCs for nonsterile column experiments. Predicted BTCs were generated using (i) the LEA model with logistic degradation kinetics and independent estimates of R_f (from $K_d = 0.66 \text{ L kg}^{-1}$), D (Table 5), X_0 (0.02 mg L^{-1}), Y (0.31) and μ_L ($0.13 \text{ L mg}^{-1} \text{ h}^{-1}$), (ii) the LEA model with first-order degradation kinetics and independent estimates of R_f , D and μ_{1b} (0.066 h^{-1}), and (iii) the LEA model with first-order degradation kinetics and independent estimates of R_f , D and μ_{1s} (calculated from C_s using Eq. [26], Table 6)	70

15. Comparison of observed 2,4-D BTC at column $RT = 16$ h, $L = 28.5$ cm, and $v = 1.5$ cm h^{-1} (experiment RT16_L28) with predicted BTCs using logistic degradation kinetics with four cases of logistic model parameters determined from batch experiments (Table 4): Case *a* - prewetted soil, water content = 0.25 L (kg soil) $^{-1}$, initial 2,4-D concentration (S_0) = 1.0 mg L^{-1} ; Case *b* - previously dry soil, water content 0.23 L (kg soil) $^{-1}$, $S_0 = 1.0$ mg L^{-1} ; Case *c* - stirred slurry, $S_0 = 1.0$ mg L^{-1} ; Case *d* - stirred slurry, $S_0 = 0.1$ mg L^{-1} . The symbols in the simulation curves correspond to those of the corresponding batch experiments in Fig. 11 73
16. First-order degradation rate constants derived from ^{14}C -2,4-D steady-state effluent concentrations as a function of column residence time (A), pore water velocity (B), and column averaged *local opportunity time*, v^{-1} (C). The curves in B and C represent best-fit empirical functions as described in the text 79

ABSTRACT

Preferential flow of water through soil macropores has been of concern because it may be a source of accelerated contaminant transport into underlying groundwater. We designed an experimental system to study effects of soil matric potential (h) on the occurrence of nonequilibrium (preferential) flow conditions in four intact cores (15 cm diameter, 30 cm length) of a permanent grassland soil. Nonequilibrium transport of a nonsorbing tracer ($^3\text{H}_2\text{O}$) was consistently observed at $h \geq -5$ cm, while equilibrium conditions were consistent at $h \leq -10$ cm. This suggests that soil pores with equivalent radii larger than 150 to 300 μm may contribute to preferential flow. However, no relationship between the soil volume occupied by macropores and preferential flow was identified. Although the onset of nonequilibrium transport was associated with increases in pore water velocity (v) within each individual soil column, no consistent dependency of the occurrence of nonequilibrium on v was observed among replicate soil columns. Since the pore water velocities associated with preferential flow observed in the current study are often exceeded under local climatic conditions, preferential flow events may be important under local field conditions.

For many organic solutes, microbial degradation is one of the most important processes controlling contaminant fate and transport. We used 2,4-dichlorophenoxyacetic acid (2,4-D) as a model compound to (i) test the applicability of first-order and logistic growth models for describing microbial degradation under batch and transport conditions, (ii) determine the applicability of batch-derived degradation parameters under a wide range of transport conditions, and (iii) separate effects of column residence time (RT) and v on degradation rate parameters. Degradation of 2,4-D under batch conditions was best described by a logistic growth model. Under transport conditions (repacked soil columns), a continuous pulse of 1 mg L^{-1} 2,4-D in the eluent solution resulted in a wide range of steady state 2,4-D effluent concentrations ($0.063\text{--}0.92 \text{ mg L}^{-1}$). Although degradation of 2,4-D under transport conditions was best described by first-order degradation kinetics, estimated first-order degradation rate constants (μ_{1s}) ranged from 0.007 to 0.071 h^{-1} as a function of v . Estimated values of μ_{1s} were not correlated with RT, but could be explained by invoking a relationship between v and a *local opportunity time* (time per unit length).

CHAPTER 1

INTRODUCTION

The introduction and misuse of anthropogenic chemicals around the globe has created serious environmental health problems. For example, in 1975, the U.S. Environmental Protection Agency (EPA) identified 154 organic compounds in drinking water supplies of towns and cities along the Ohio, Potomac, and Mississippi rivers. The source of these chemicals included industrial and municipal discharges, accidental spills, runoff from agricultural and urban areas, and chlorination processes at water treatment plants (Sparks, 1993). In 1990, the U.S. EPA published a survey of pesticides and nitrates in community and well water supplies. About 10% of the community water supplies and 4% of the rural water wells had detectable concentrations of pesticides. More than 50% of the wells had detectable nitrate concentrations (Carey, 1991). Unfortunately, we are often not able to predict if a chemical released into the environment will cause pollution or not. Detrimental effects of chemicals on biological species can be complex, long-term and spatially variable. Environmental scientists are challenged to elucidate this complexity and to suggest management practices or alternatives which minimize and ideally eliminate pollution. In fact, the U.S. National Research Council identified the reduction of adverse impacts of chemicals in the environment to be one of six research areas that are most vital

to society within the coming 20-25 years (National Research Council, 1996; Glaze, 1997).

Inevitably, soil and water are major sinks for many pollutants. Agricultural fertilizers resulting in increased levels of phosphates and nitrates in soils may cause eutrophication of surface waters and contribute to the degradation of groundwater resources. Many pesticides used to control weed species, invertebrate pests, and plant pathogens in both agricultural and residential systems have been found in groundwater. Acid rain deposition has caused deforestation of significant areas in Central Europe. Trace metals, introduced from sewage sludge, industrial wastes, or mining tailings often have toxic effects on organisms living in or on soil. As of 1992, more than 28,000 hazardous waste sites were present in the United States and 1177 contaminants were on the National Priority Superfund List (Yong et al., 1992).

With increasing concern over soil and water contamination, interest in predicting the fate and transport of chemicals in soils has grown rapidly over the last two decades. However, there is considerable uncertainty regarding the long-term fate of chemicals in soils. This uncertainty is due, in part, to our limited ability to describe the complexity and heterogeneity of soils, and to the difficulty of integrating chemical, biological, hydrological and atmospheric processes. Under these constraints, simplified models, which have been derived under idealized and isolated conditions, are usually combined to predict more complex processes of transformation and transport of chemicals in soils (Carsel et al., 1984; Nofziger and Hornsby, 1987; Steenhuis et al., 1987; Knisel et al., 1989; Wagenet and Hutson, 1987).

The movement of chemicals through soil is often modeled as transport through a homogeneous porous medium using mean advective transport superimposed with random dispersion (advection-dispersion model; Jury and Flühler, 1992). It is, however, well known that homogeneity is a valid assumption only under certain soil conditions, such as exist in structureless soils with little pore size heterogeneity. Consequently, it is not uncommon for these models to fail under nonideal soil and hydraulic conditions present in many field situations. Water flow through soils may occur preferentially through large pores caused by biological activity or along structural boundaries, essentially bypassing a significant volume of the soil matrix. Under preferential flow conditions, spatially variable pore water velocities can result in rapid movement and early arrival of solutes, which is not consistent with model descriptions based on equilibrium advective-dispersive transport. For example, in one field study on the transport of napropamide through sprinkler-irrigated Etiwanda sandy loam soil, the mean predicted depth of napropamide was about 13 cm, whereas traces of the compound were found as deep as 190 cm (Clendening and Jury, 1990). On the same site, triallate reached 100 cm with the application of 5 cm of water, whereas the mean predicted depth of leaching was only 3 mm for this strongly sorbing compound. The accelerated breakthrough of chemicals caused by preferential flow has serious implications for the contamination of groundwater, because transformation rates are often lower below the biologically active soil zone and chemicals persist longer. It is well known that preferential flow through structured soils occurs primarily when the soil is saturated, and is often unimportant under unsaturated conditions. There is, however, a lack of information on the transition

from preferential flow to matrix flow with changing soil hydraulic conditions. One of the goals of the current study was to identify soil hydraulic conditions associated with preferential flow. Specific objectives under this goal included the investigation of effects of soil matric potential (h) and pore water velocity (v) on the occurrence of preferential flow through intact soil cores from native and tilled sites. Results from this study (Chapters 2 and 3) may be used to assist in the identification of field conditions under which preferential flow events are likely to occur.

Another important process controlling the fate and transport of contaminants through soils is microbial degradation. Numerous kinetic models have been proposed for describing microbial degradation rates of chemicals in soils under well-controlled batch conditions. Only a few studies exist, however, where the performance of these models has been critically examined under transport conditions, which are typical of field soils. Because of its simplicity, the first-order kinetic expression has been used in the majority of fate and transport models for describing microbial degradation during transport (Pennell et al., 1990). However, there are many instances documented in the literature where first-order kinetics are unsuitable for describing contaminant degradation in soils (Alexander and Scow, 1989). Furthermore, independent of the model used to describe microbial degradation during transport, there is uncertainty regarding the appropriate choice of rate parameters necessary for predicting degradation. Some studies suggest that rate parameters obtained under batch conditions may not be appropriate under transport conditions (Estrella et al., 1993), and further that rate parameters may depend on the solute flow regime (Kelsey and Alexander, 1995). If this is generally true, then our ability

to predict the degradation of organic chemicals under a wide range of transport conditions using a single set of rate parameters is reduced significantly. Increasing residence times of chemicals in soil will generally result in increasing amounts of the chemical degraded. This is consistent with first-order degradation kinetics. However, there is little published information concerning potential effects of pore water velocity (v) on apparent degradation rate parameters observed during transport. Since most experiments employ constant column lengths, changes in residence time are generally associated with changes in v and vice-versa. Therefore, a second goal of this thesis was to investigate the influence of varying transport conditions on the degradation behavior of an organic chemical. Specific objectives included (i) to test the applicability of first-order and logistic growth models for the description of 2,4-D (2,4-dichlorophenoxyacetic acid) degradation across a wide range of transport conditions, (ii) to determine the applicability of degradation rate parameters derived under batch conditions for describing 2,4-D degradation across a wide range in column conditions, and (iii) to separate effects of column residence time and pore water velocity on degradation rate parameters determined from transport experiments.

CHAPTER 2

APPARATUS FOR CONSTANT-POTENTIAL SOLUTE TRANSPORT AND SOIL WATER CHARACTERISTIC DETERMINATION

INTRODUCTION

Many investigations concerning unsaturated soil water or chemical movement require imposition of steady (or near-steady) state hydraulic conditions. This is generally addressed by controlling the rate of solution inflow (e.g., van Genuchten and Wierenga, 1986; Gaber et al., 1995) or by applying a constant negative supply pressure to the inlet end of the soil column during infiltration (e.g. Nielsen and Biggar, 1961; Seyfried and Rao, 1987; Munyankusi et al., 1994; Magesan et al., 1995, Vogeler et al., 1996). While an advantage of the first approach is ease in switching between eluent sources, the latter facilitates setting a desired matric potential (h) at the column inlet. Negative pressure at the base is often achieved by placing the soil column on a porous plate (e.g., stainless steel or ceramic) through which a known vacuum may be applied. If equal negative pressure is applied to the top and bottom of the column, the overall hydraulic potential energy gradient along the vertical column is unity. In a homogeneous porous medium, this will result in a uniform, steady state matric potential with water flow driven by the unit gradient gravitational potential only. However, soil columns will often deviate from

unit gradient because of heterogeneities in the pore system with depth; this is particularly true for intact or "undisturbed" soils. Pore discontinuities at the interface of the porous plate and soil which result in low interfacial hydraulic conductivity may also interfere with establishment of unit gradient within soil cores. In this situation, effects of a drop in h above the porous bottom plate can potentially be avoided by measuring h within the core and adjusting the bottom plate suction. Failure to achieve or to maintain constant potential steady flow conditions in soil columns will result in inaccurate or inappropriate results and conclusions.

Another common problem during soil column leaching experiments involves changes in soil properties during the course of an investigation (e. g., Vandevivere and Baveye, 1992). Continuous monitoring of θ and h can alert an investigator to changes in the $\theta(h)$ relationship that may affect experimental results.

We designed and tested a system to impose, maintain, and monitor uniform soil matric potential during miscible displacement experiments in large intact soil cores. In addition, during column conditioning (sequential wetting and drying) a detailed soil water characteristic relationship may be determined in situ by simultaneous measurements of θ and h using time domain reflectometry (TDR) and pressure transducer tensiometry (Wraith and Baker, 1991; Hudson et al., 1996). Novel aspects of our approach include an effective means to ensure that unit gradient flow conditions are established and maintained, simultaneous collection of large effluent volumes without interruption of the outlet pressure, and continual monitoring of column $\theta(h)$ during the course of single or multiple experiments. This paper describes the system for constant-potential solute

transport and $\theta(h)$ determination, discusses some of its advantages and disadvantages compared with conventional approaches, and briefly illustrates its application to monitoring and evaluating miscible displacement of tritiated water in large intact soil cores.

While not specifically addressed in this paper, the system described here may also be used to quantify the column hydraulic conductivity $[K(\theta)]$ relations (e.g., Hussen et al., 1994), and/or to monitor the movement of ionic solutes using TDR (Wraith et al., 1993; Vogeler et al., 1996; Risler et al., 1996), under controlled and well-characterized column transport conditions.

MATERIALS AND METHODS

We obtained intact soil cores (15.2 cm diameter, 30 cm length) from the A. H. Post Experimental Farm near Bozeman, MT by forcing beveled and lubricated PVC pipe into the soil using a hydraulic core sampler. Soils at this location are classified as Amsterdam silt loam (fine-silty, mixed Typic Haploboroll). Transducer tensiometers (0.6 cm width, 6.5 cm length high-flow ceramic cups, Soil Moisture Equipment Co., Santa Barbara, CA; model 141PCG sensors, Micro Switch, Freeport, IL), fabricated in our laboratory, were horizontally inserted in the column at depths of 9 and 21 cm (Fig. 1) and connected to a data logger (model 21X, Campbell Scientific, Logan, UT). Pressure transducers were individually calibrated using a water manometer. A 10-cm long 3-rod TDR waveguide (Midwest Industries, St. Paul, MN) was installed normal to each tensiometer and was offset by about one centimeter vertical distance.

A modified disk permeameter (Perroux and White, 1988) base allowed eluent to be

applied at the top of columns under controlled ponded or negative supply pressure (Fig. 1). Air entry pressure of the permeameter membrane was about 30 cm. One 3-way and

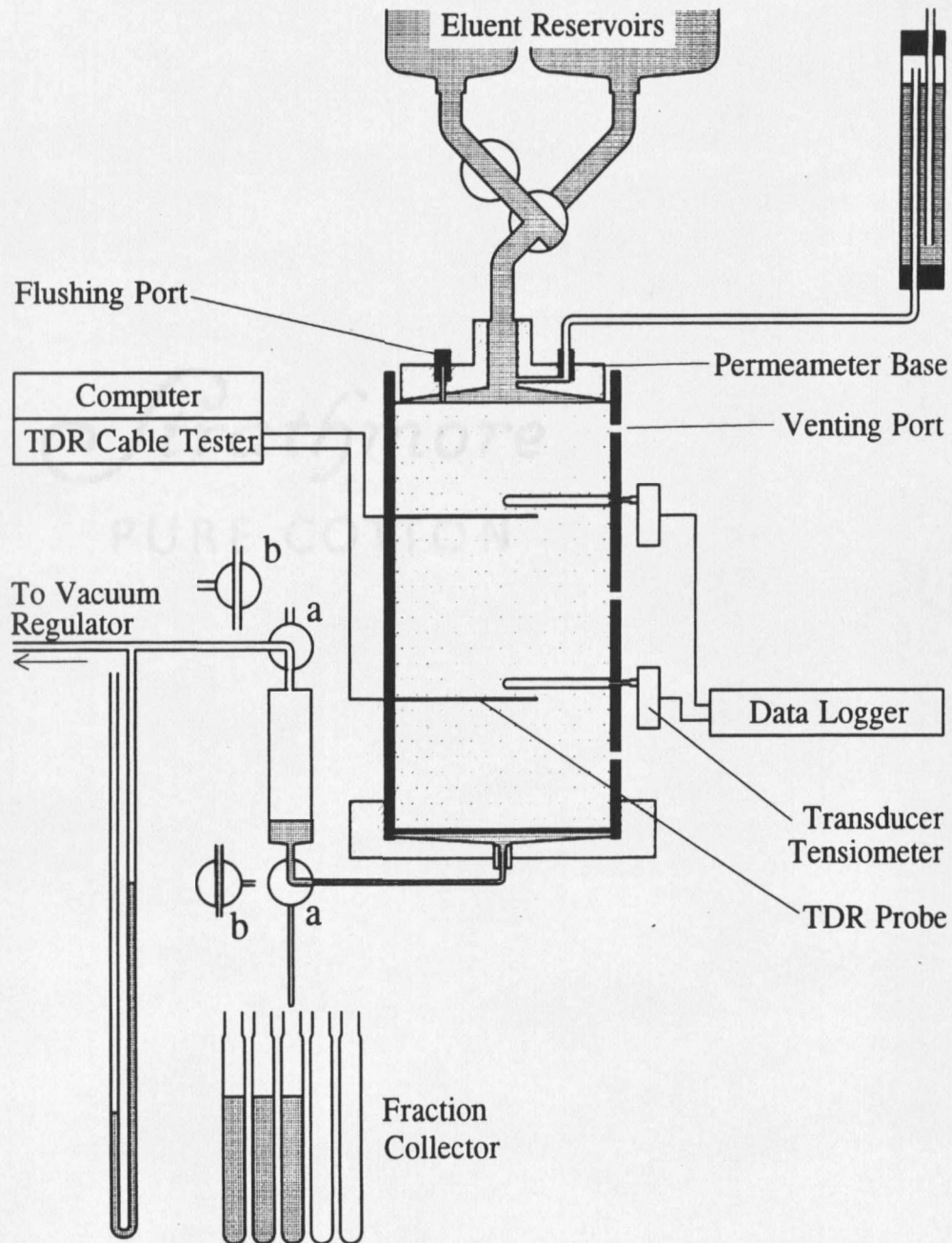


Figure 1. Schematic diagram of soil column control and monitoring system with valves in collecting mode (a) and sampling mode (b).

one 2-way valve (Elliptic Valves ½" NPT, Cole Parmer Instrument Co., Niles, IL) connected in series allowed switching between different eluent solutions. Switching eluents by replacing the permeameter (Magesan et al., 1995) was not feasible with our test soil because of mechanical damage of the soil surface layer and subsequent changes in the soil column hydraulic characteristics. All solution inlet lines that simultaneously transmitted liquid and air required a flow diameter of at least 1.0 cm to allow free opposite movement of the phases, or air and solution lines needed to be separated, e.g. by inserting a smaller air tube into a larger liquid-filled tube. The permeameter was equipped with a flushing port similar to that of Seyfried and Rao (1987) which facilitated rapid exchange of eluent sources without measurable supply pressure fluctuation. To switch between eluent solutions, the valve connecting to the eluent reservoir was closed. Then, a pressure slightly lower than the pressure set with the Mariotte Device was applied to the flushing port and the appropriate valve to the new reservoir was slowly opened. To minimize mixing of eluent solutions within the permeameter foot, the valve controlling the new eluent reservoir was opened and closed several times while solution was continuously removed through the flushing port. The radius of the infiltrometer base was about 0.5 centimeter less than that of the soil surface, allowing air exchange as the column was wetted or drained. Additional air entry ports at several depths in the column wall did not appear to affect wetting and draining and were omitted after preliminary studies. To ensure good contact between the soil and infiltrometer membrane, we severed any above-ground vegetative residue, slightly leveled the soil surface if necessary, and added a 1-cm layer of graded fine silica sand (Grade 70 sieved through 149 µm screen).

The column base was designed to allow simultaneous application of negative pressure and collection of large effluent volumes without interruption of pressure at the column base. The lower surface of the soil rested on a porous stainless steel plate (Mott Metallurgical Corp., Farmingdale, CT) with an air entry pressure of 300 cm and was sealed with rubber O-rings in an acrylic endcap. Outlet pressure was controlled by a vacuum regulator (model 44-20, Moore Products Co., Spring House, PA) and measured with a water manometer. Column effluent was stored in a glass reservoir between two 3-way solenoid valves (model B14DK1030, Skinner Valve Div., New Britain, CT) during collection mode (position "a" in Fig. 1). After tubes advanced in the fraction collector (Retriever II, ISCO, Lincoln, NE) under the column, a timed controller switched the valves to sampling mode (position "b") and allowed the collected effluent to rapidly drain into a sample tube. The solenoid valves were set back to the collection position about 10 s later. Pressure fluctuations during a collection/sampling cycle were dependent on the amount of liquid in the glass reservoir. Since the net bottom plate pressure was offset from the pressure at the vacuum regulator by the height of the water column in the collection reservoir, we noted fluctuations in h of 1 to 2 cm at the lower tensiometer. These fluctuations could be reduced by shortening the collection cycle and thus reducing the depth of water in the reservoir. However, this would increase the number of sampling tubes collected. A reservoir with wider diameter thus seems a likely solution to this issue.

Measurement of Soil Water Characteristic

The soil water characteristic relationship (Fig. 2) was measured for the instrumented soil columns by simultaneously monitoring soil matric potential and volumetric water content during preliminary column wetting and drying cycles (Wraith and Baker, 1991). During wetting to saturation, a 3 mM CaCl₂ solution was incrementally added from the column base over a period of at least 72 h. The water retention curve was measured by first draining the soil column at $h = 0$ for 24 h. The effluent collected during this cycle was used to calculate drained porosity (Kluitenberg and Horton, 1990; data not shown). Additional soil water was then removed by stepwise application of tension (to -200 cm) at

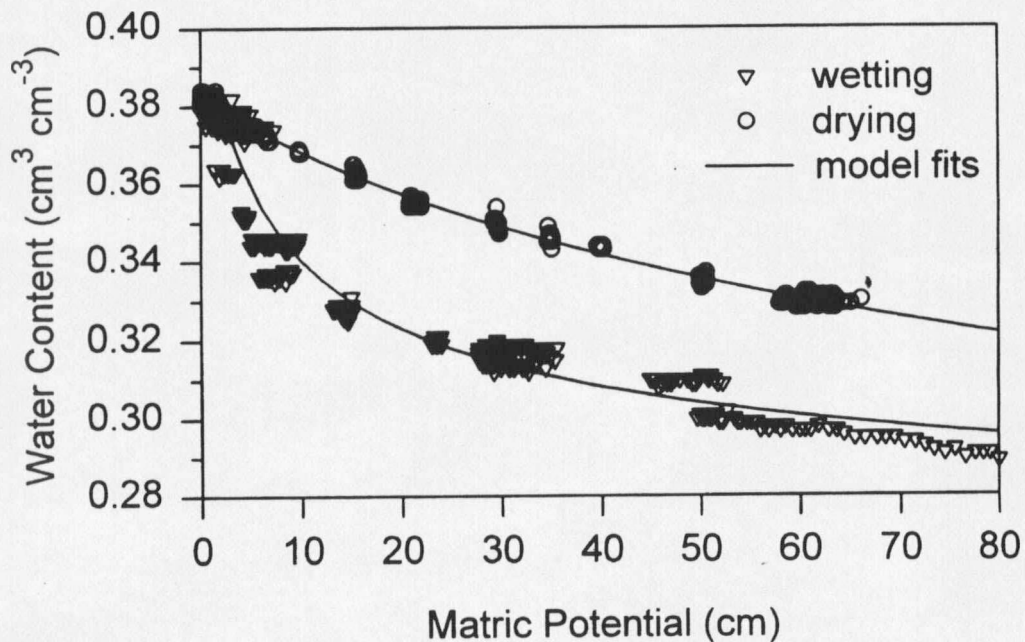


Figure 2. Experimental wetting and drying curves for one TDR waveguide-tensiometer pair. The wetting and drying limbs were individually fit to the van Genuchten (1980) model.

the bottom plate. Paired h and θ readings, taken at least one hour after each water addition or removal step (i.e., after establishing quasi-static conditions; Vachaud et al., 1972), were used to fit a model describing $\theta(h)$ (van Genuchten, 1980) using nonlinear least squares optimization. Tensiometer readings were compensated for the difference in elevation between tensiometer cups and TDR probes.

Setting Unit Potential Gradient

Following wetting from the base, the disk permeameter supply pressure was adjusted to the desired column matric potential (h). Increasingly negative pressure was then applied at the base until the top and bottom tensiometer readings were equal, i.e., unit gradient conditions had been reached. Achieving equivalent top and bottom tensiometer readings usually required the bottom plate pressure to be 5 to 25 cm lower than the target column h value. We were able to maintain measured deviations from the target h value to less than 1 cm for complete transport experiments lasting one or two weeks. Due to alteration in soil pore arrangement during transport experiments, tensiometer and TDR readings sometimes changed over time. Periodic adjustment of the bottom plate pressure on the order of fractions of a centimeter to several centimeters were necessary to maintain constant matric potential throughout an experiment. These adjustments were required at intervals of several days at $h < -10$ cm, and every few hours at h between -2 and -5 cm. We were not able to establish $h = 0$ throughout a soil column for sufficient periods of time to complete transport experiments because of soil column heterogeneities. Saturated solute transport experiments were therefore performed at a permeameter pressure of zero

and bottom plate pressures of -50 cm, which resulted in positive pressure at the tensiometers. Our system design was restricted to the range between ponding and $h = -25$ cm, with the limiting factor being the air entry pressure of the disk permeameter membrane. Use of finer mesh or alternative materials would extend this range.

Monitoring Column Hydraulic Conditions

It is often desirable to conduct multiple transport experiments using the same soil core because of variability in physical attributes among individual cores. However, alteration of the pore system caused by physical/chemical effects of hydration, particle movement, or microbial growth can create substantial problems during repeated wetting and drying or prolonged exposure to high wetness. Figure 3 illustrates that combined continuous measurement of water content and matric potential during our transport experiments facilitated identification of a gradual change in the $\theta(h)$ relationship. Increasing water content at a constant $h = -24$ cm indicated the filling of previously drained soil volumes. Figures 4a and 4b show measured soil matric potential and water content at two heights during a solute transport experiment at $h = -5$ cm. The tensiometer readings were periodically checked and the bottom plate suction adjusted as needed during the course of the experiment. We have also successfully used the experimental control and monitoring system to study the effects of matric potential (h) on the occurrence of nonequilibrium transport in intact soil cores during steady unit gradient saturated and unsaturated water flow (Langner et al., 1994). Two to four transport experiments with transport of six pore volumes each were generally possible with a single soil column before significant

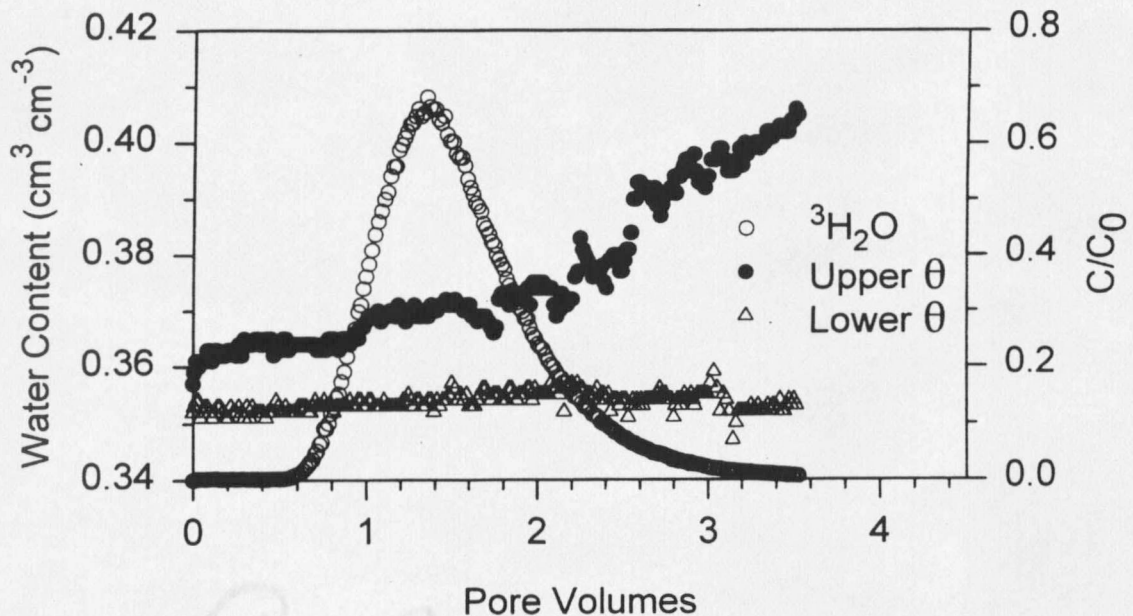


Figure 3. Measured soil water content (θ) during a $^3\text{H}_2\text{O}$ miscible displacement experiment at $h = -24$ cm. Upper and lower θ refer to two TDR probe positions in the intact soil column. Increasing θ indicates gradually degrading pore system in the upper layer of the core after two previous leaching experiments (approximately 10 pore volumes) with insignificant changes.

changes of the pore systems were observed. Similarly, continuous monitoring of the soil matric potential explained observed anomalies in some BTCs.

The preliminary quantification of the soil water characteristic shortened the usable life of soil cores for subsequent transport studies. After generating a complete water characteristic in the range $h = 0$ to -70 cm, we were able to run only two to three transport experiments (6 pore volumes per experiment) on the same soil core. In cores where we did not characterize $\theta(h)$ we did not observe significant alteration of the apparent soil pore size distribution until after the fourth transport experiment.

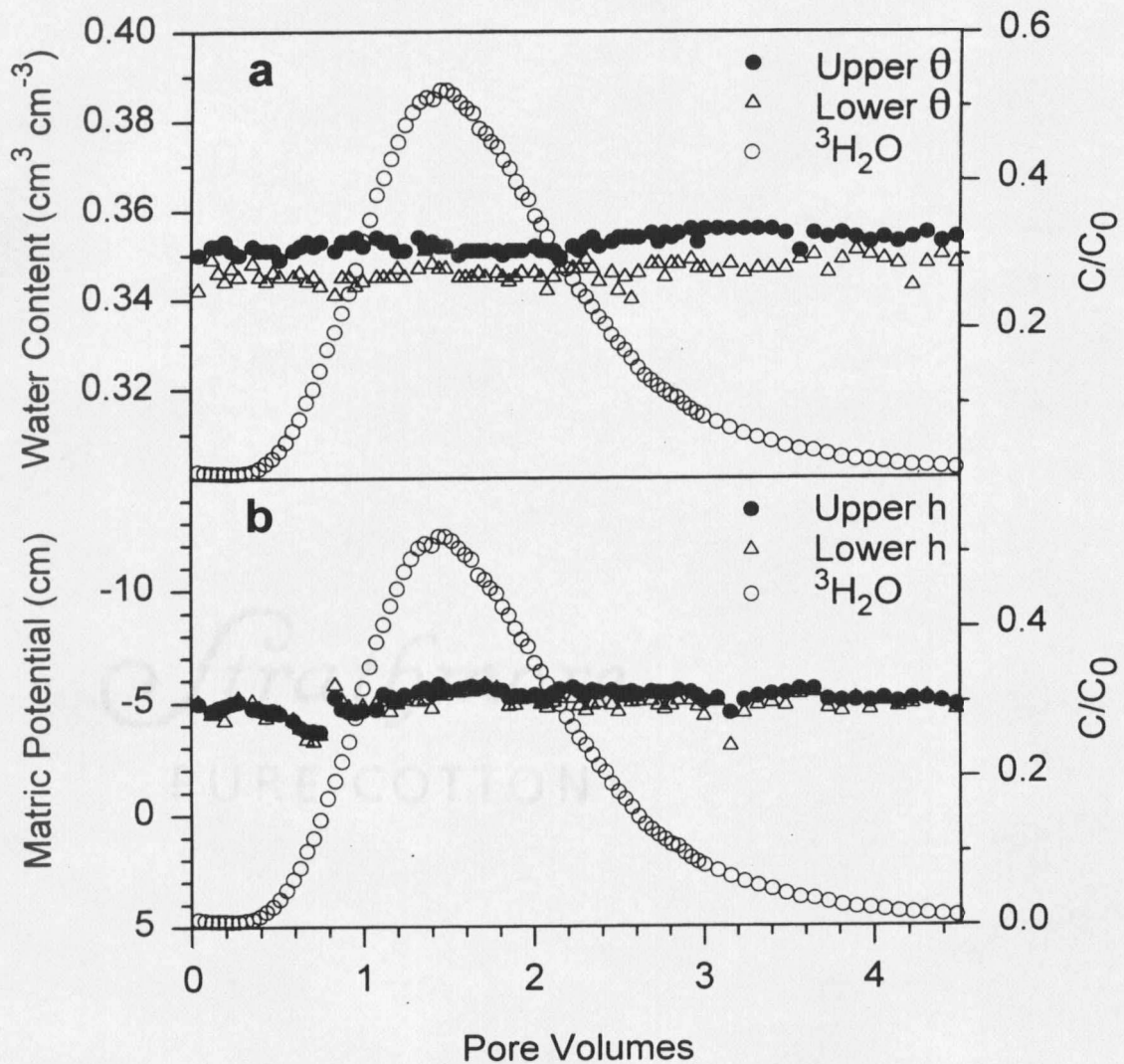


Figure 4. Measured soil water content (a) and soil matric potential (b) during a $^3\text{H}_2\text{O}$ miscible displacement experiment at $h = -5$ cm. Upper and lower θ or h refer to two TDR probe or tensiometer positions in the intact soil column. The irregularity in h at about 0.7 pore volumes indicates slight flow disruption during switching of eluent from pulse to background solution.

CHAPTER 3

PREFERENTIAL FLOW THROUGH INTACT SOIL CORES: EFFECTS OF MATRIC POTENTIAL

INTRODUCTION

Numerous studies have shown that water and solutes can move through soil along preferred pathways, bypassing much of the soil matrix (Ehlers, 1975; Quisenberry and Philips, 1976; Kanwar et al., 1985; Rice et al., 1986; Wagenet, 1987; Seyfried and Rao, 1987). Such transport behavior is known as channel, bypass, or preferential flow (Singh and Kanwar, 1991), and has been identified as a major cause of groundwater contamination by agrichemicals (Jaynes et al., 1995). Preferential flow can result in rapid solute movement into the vadose zone or to groundwater where it is common to observe lower microbial degradation rates that result in increased persistence.

Due to its potential importance in impacting the fate of agrichemicals, preferential flow has been studied intensively during the past two decades. Numerous studies have evaluated the dependence of preferential flow on soil macroporosity (Germann and Beven, 1981; Luxmoore et al., 1990; Li and Ghodrati, 1994) or on management practices (e.g., tillage or application of manure) which influence soil macroporosity (Singh and

Kanwar, 1991; Wu et al., 1995; Munyankusi et al., 1994). Results indicate that preferential flow is generally correlated with the number or volume of soil macropores. Although it is well recognized that the potential for preferential water and solute flow will increase with increases in macroporosity, it has been difficult to determine relationships among specific properties of soil pores (especially pore sizes) and the susceptibility to preferential flow.

Germann and Beven (1981) have suggested that the minimum radius of macropores (i.e., pores potentially forming preferential flow paths) is 1.5 mm, while Luxmoore (1981) defined macropores as pores > 0.5 mm. In one transport study using undisturbed cores of an aggregated tropical soil, Seyfried and Rao (1987) observed significant preferential flow at matric potentials (h) of 0 and -1 cm; when h was lowered to -10 and -20 cm, no preferential flow was observed. This suggests that pores with equivalent radii smaller than 0.150 mm (water-filled at $h = -10$ cm) did not contribute to preferential flow in their test soil. Other suggestions of macropore sizes range from >0.005 to >1.5 mm [see tables in Beven and Germann (1982) and Luxmoore et al. (1990)]. Although factors other than pore size (such as pore structure and pore continuity) undoubtedly influence the potential for preferential flow (Bouma, 1990; Logsdon et al., 1993), the wide range in estimated macropore radii is due partly to our inability to identify water-conducting pore sizes responsible for preferential flow events. To narrow this range, experiments would be necessary where (i) the water content (drained or filled) of various pore size fractions in the soil can be effectively controlled, and (ii) simultaneously, the transport behavior of solutes can be tested for the presence of preferential flow conditions.

Preferential flow can often be interpreted as a nonequilibrium transport process, where the soil profile may contain discrete water domains or regions. While one-region models assume a homogeneous pore water velocity throughout the porous medium, two-region models divide the porous medium into a *mobile* domain, where solute transport occurs by advection and dispersion, and an *immobile* domain, in which there is minimal advective flow (van Genuchten and Wierenga, 1976). Rapid transport in the mobile domain is accompanied by diffusive mass transfer of solutes between mobile and immobile regions. Because diffusive mass transfer rates may constrain equilibrium between the immobile and the advective domains, solutes in the system may be considered to be in a state of nonequilibrium. This phenomenon has been termed transport or physical nonequilibrium (PNE; Brusseau and Rao, 1990; van Genuchten and Wierenga, 1976). When preferential flow conditions are present, a two-region (or PNE) model will generally fit the observed solute breakthrough data better than a one region (or local equilibrium) model. In the absence of preferential flow, the PNE model reduces to a local equilibrium model.

The primary objective of the present study was to examine soil matric potentials and corresponding pore sizes associated with nonequilibrium transport in naturally structured soils. Tracer transport experiments through large intact soil cores were performed at several matric potentials, and the observed BTCs were analyzed for physical nonequilibrium using a comparison between fitted local equilibrium and physical nonequilibrium models.

MATERIALS AND METHODS

Soil

Intact soil cores (15.2 cm diameter, 30 cm length) were obtained at the A. H. Post Experimental Farm near Bozeman, MT from a permanent grassland site. Soils at this location are classified as Amsterdam silt loam (fine-silty, mixed Typic Haploboroll). A hydraulic core sampler was used to force beveled and lubricated PVC pipe into the moist (approximate field capacity) soil. Cores were carefully excavated and stored upright in sealed plastic bags at 4°C prior to their use in leaching experiments. Large numbers of vertical wormholes and root channels were visible at both ends of the soil cores (e.g., >20 tubular pores with radii > 1 mm).

Experimental Setup

The preparation of soil cores and the experimental column apparatus were described in detail in Chapter 2 of this thesis. The soil columns were used for both the generation of soil water characteristics [$\theta(h)$ relationship] and for performing unit gradient solute transport experiments. Soil cores were equipped with transducer tensiometers and TDR waveguides at two depths (about 8 and 20 cm) within the column. A modified disk permeameter was used to deliver eluent solutions to the top of the column. The column bottom rested on a porous stainless steel plate allowing uninterrupted application of constant negative pressure as well as collection of large volumes of effluent.

Transport Experiments

A series of 2 to 4 transport experiments under steady-state hydraulic conditions was performed with each of 4 undisturbed soil cores. The matric potential (h) was varied between experiments with identical soil columns. The primary goal was to obtain breakthrough curves (BTCs) of $^3\text{H}_2\text{O}$ and pentafluorobenzoic acid (PFBA) at a minimum of three matric potentials per column. Across all columns, matric potentials ranged from $h = 0$ (ponding, column experiments PN12_2 and PN11_1) to $h = -24$ cm (PN14_4).

Soil columns were gradually saturated from the bottom over a period of 2 d using 3 mM CaCl_2 . Following saturation, the disk permeameter supply pressure was adjusted to deliver 3 mM CaCl_2 at the desired column matric potential. Increasingly negative pressure was then applied to the porous plate at the column base until the top and bottom tensiometer readings were equal. To ensure approximate unit gradient conditions within the soil column (i.e., equal tensiometer readings at both positions within the column) the bottom plate pressure had to be adjusted to between 5 and 25 cm lower than the target column h value. Pressure transducer tensiometer readings were periodically checked throughout the experiments and the base pressure was adjusted if necessary to account for temporal drift in h resulting from changes in pore arrangement within the soil core (Chapter 2, p. 13).

Unit gradient hydraulic conditions could not be established at $h = 0$ because of insufficient flow rate through the bottom porous plate. In an attempt to overcome flow limitations through the porous plate under saturated conditions, we conducted a preliminary experiment where the plate pressure was decreased until the tensiometer readings

were zero. However, we were not able to establish steady-state flow conditions within the column and a very irregular BTC (not shown) was obtained. Saturated solute transport experiments were therefore performed at disk permeameter pressures of zero and bottom plate pressures of -50 cm, which resulted in positive pressures at the tensiometer locations.

After steady state hydraulic conditions had been established, the eluent was switched to a pulse solution containing 3 mM CaCl₂, ³H₂O (specific activity, 1.67 x 10⁵ Bq L⁻¹, Sigma Chemical Co., St. Louis, MO), and 0.1 g L⁻¹ PFBA (Sigma Chemical Co.). Eluent was switched back to 3 mM CaCl₂ when approximately 0.7 pore volumes of pulse solution had been applied. Experiments were continued for 4 pore volumes, after which the column was resaturated and reconditioned for subsequent transport experiments at different levels of *h*. Two to four transport experiments were generally possible with a single soil column before significant changes in hydraulic conductivity and $\theta(h)$ indicated changes of the pore systems of the soil cores (Chapter 2, p. 14).

Effluent fractions were analyzed for ³H₂O using a Packard 2200CA liquid scintillation analyzer (Packard Instrument Co., Downers Grove, IL) and for PFBA using a Dionex 4000i ion chromatograph (Dionex Corp., Sunnyvale, CA; Dionex AS4A column).

Modeling

Solute BTCs were evaluated using two forms of the advection-dispersion equation (ADE) as a mechanism for identifying the presence or absence of physical nonequilibrium: (i) the local equilibrium assumption (LEA), and (ii) a two-region physical

nonequilibrium (PNE) model (Toride et al., 1995).

Local Equilibrium Assumption

The advection dispersion equation (ADE) used to describe one-dimensional transport of a sorbing solute under steady-state fluid flow conditions through homogeneous porous media is given by (Lapidus and Amundson, 1952)

$$\frac{\partial c}{\partial t} + \frac{\rho}{\theta} \frac{\partial s}{\partial t} = D \frac{\partial^2 c}{\partial x^2} - v \frac{\partial c}{\partial x} \quad [1]$$

where c is the solution-phase solute concentration (e.g., mg L^{-1}), t is time (h), ρ is soil bulk density (kg L^{-3}), θ is volumetric water content ($\text{m}^3 \text{m}^{-3}$), s is sorbed-phase solute concentration [mg kg^{-1}], D is the hydrodynamic dispersion coefficient ($\text{cm}^2 \text{h}^{-1}$), x is the distance from solute application (cm), and v is the average pore water velocity (cm h^{-1}). Assuming conditions of sorption-desorption equilibrium throughout the soil profile, isotherm singularity and linearity [$s = K_d c$, where K_d is the linear equilibrium sorption coefficient (L kg^{-1})], the $\partial s/\partial t$ term becomes $K_d \partial c/\partial t$, and Eq. [1] may be simplified:

$$R_f \frac{\partial c}{\partial t} = D \frac{\partial^2 c}{\partial x^2} - v \frac{\partial c}{\partial x} \quad [2]$$

where $R_f = 1 + (\rho/\theta)K_d$ is the retardation factor. The LEA model (Eq. [2]) may be written in nondimensional form (Brusseu and Rao, 1989)

$$R_f \frac{\partial C}{\partial T} = \frac{1}{P} \frac{\partial^2 C}{\partial X^2} - v \frac{\partial C}{\partial X} \quad [3]$$

with the dimensionless parameters defined as follows

$$C = \frac{c}{c_0} \quad [4]$$

$$P = vL/D \quad [5]$$

$$T = vt/L \quad [6]$$

$$X = x/L \quad [7]$$

where C is the relative solute concentration, c_0 is the eluent solute concentration (mg L^{-1}), P is the Peclet number describing the shape of the solute BTC (i.e., relative magnitude of dispersion), L is column length (cm), T is dimensionless time (i.e., pore volumes) and X is dimensionless distance.

Physical Nonequilibrium

The LEA model (Eq. [2]) does not appropriately describe solute transport under conditions where macropores form preferential flow paths, which result in significant heterogeneities in pore water velocity (v). Substantial spatial variation in v can affect the

transport of sorbing and nonsorbing solutes, and its results have generally been described as physical nonequilibrium (PNE) or transport-related nonequilibrium (van Genuchten and Wierenga, 1976; Brusseau et al., 1989). Van Genuchten and Wierenga (1976) modified the ADE to explicitly differentiate two soil water regions where all advective-dispersive transport is assumed to occur in the mobile region, and transport in the immobile region is restricted to diffusion. Again, sorption-desorption is assumed to be an equilibrium process following a linear, singular isotherm. The governing differential equations for this model (referred to here as the PNE model) are given as

$$(\theta_m + f\rho K_d) \frac{\partial c_m}{\partial t} + [\theta_{im} + (1-f)\rho K_d] \frac{\partial c_{im}}{\partial t} = \theta_m D \frac{\partial^2 c_m}{\partial x^2} - v_m \theta_m \frac{\partial c_m}{\partial x} \quad [8]$$

$$[\theta_{im} + (1-f)\rho K_d] \frac{\partial c_{im}}{\partial t} = \alpha (c_m - c_{im}) \quad [9]$$

where θ_m and θ_{im} are mobile and immobile volumetric water contents, respectively ($\text{m}^3 \text{m}^{-3}$), $\theta_m + \theta_{im} = \theta$, c_m and c_{im} are solution-phase solute concentrations in the mobile and immobile regions, respectively (mg L^{-1}), f is the fraction of sorption sites that equilibrate with the mobile region, v_m is the average pore water velocity in the mobile region (cm h^{-1}), and α is the first-order mass transfer coefficient between the two regions (h^{-1}). In analogy to the LEA model (Eq. [2]), the PNE model (Eq. [8] and [9]) may be written in nondimensional form

$$\beta R_f \frac{\partial C_m}{\partial T} + (1 - \beta) R_f \frac{\partial C_{im}}{\partial T} = \frac{1}{P} \frac{\partial^2 C_m}{\partial X^2} - \frac{\partial C_m}{\partial X} \quad [10]$$

$$(1 - \beta) R_f \frac{\partial C_{im}}{\partial T} = \omega (C_m - C_{im}) \quad [11]$$

where in addition to Eq. [5] - [7] the following dimensionless parameters are defined

$$C_m = \frac{c_m}{c_0} \quad [12]$$

$$C_{im} = \frac{c_{im}}{c_0} \quad [13]$$

$$\beta = \frac{\theta_m + \rho f K_d}{\theta + \rho K_d} \quad [14]$$

$$\omega = \frac{\alpha L}{\theta_m v_m} \quad [15]$$

where C_m and C_{im} represent relative solute concentrations in the mobile and immobile regions, respectively. The variable β is a partition coefficient describing the fraction of sorption in the mobile region (Brusseau and Rao, 1989). For nonsorbing solutes ($K_d = 0$), β reduces to the fraction of mobile water (θ_m/θ). The parameter ω is a dimensionless rate

coefficient describing the mass transfer between the mobile and immobile regions. For nonsorbing solutes such as $^3\text{H}_2\text{O}$, values of β and ω can be used to evaluate potential contributions from physical nonequilibrium. For reactive (sorbing) solutes, effects of both sorption nonequilibrium and PNE may be confounded in the fitted values of β and ω (van Genuchten, 1981; Parker and van Genuchten, 1984; Brusseau et al., 1989). Physical equilibrium conditions are approached when θ_m and f approach θ and 1, respectively, and β approaches 1. When $\beta = 1$, the PNE model (Eq. [10] and [11]) reduces to the LEA model (Eq. [3]). Similarly, if the mass transfer parameter ω in Eq. [11] increases, the rate of convergence of C_m and C_{im} increases. In the limit $\omega \rightarrow \infty$, $C_m = C_{im}$ because solutes in each domain mix instantaneously, and the PNE model again reduces to the LEA model. Several researchers have shown that optimized values of $\omega \geq 100$ indicate the absence of nonequilibrium conditions (Valocchi, 1985; Bahr and Rubin, 1987).

Estimating Transport Parameters from Breakthrough Curves

To distinguish between local equilibrium vs PNE conditions, results from miscible displacement experiments were analyzed using both LEA and PNE models. Model parameters L and v ($q\theta^{-1}$) were obtained from direct measurement where the solute flux, q (cm h^{-1}), was calculated for each experiment from the steady-state effluent flow rate, and the volumetric soil water content, θ , was determined by averaging the measured volumetric water content (TDR) at both instrumented positions. Observed $^3\text{H}_2\text{O}$ BTCs were fit to the LEA model under flux type boundary conditions using CXTFIT2, a least squares parameter optimization method (Toride et al., 1995). Values of P and R_f were optimized

for the low- h experiments (-10 to -24 cm) of each column. Batch experiments performed to assess sorption of $^3\text{H}_2\text{O}$ to the Amsterdam soil suggested that $^3\text{H}_2\text{O}$ was not sorbed (data not shown), providing justification for fixing $R_f = 1$ in the transport model optimizations. However, model fits using $R_f = 1$ did not yield reasonable agreement between observed and fitted data, which is consistent with observations of previous studies (e.g., Gaber et al., 1995; Seyfried and Rao, 1987; Wierenga et al., 1975). Therefore, R_f was optimized for the low- h experiment of each column, resulting in R_f values between approximately 1.2 and 1.4. This is justified by the fact that PNE was not observed in any of these experiments (shown below). The estimated values of R_f for low- h experiments were then used as fixed parameters for fitting $^3\text{H}_2\text{O}$ effluent data from experiments at higher h , where P was the only parameter optimized. Tritiated water BTCs were also fit using the PNE model where fitted parameters included P , β , ω and R_f (again, R_f only fitted for the low- h experiments).

The same method was applied to test for the presence of PNE using the PFBA breakthrough curves. Optimized R_f values for PFBA ranged from 0.84 to 1.00 indicating slight anion exclusion. Results concerning the presence or absence of PNE conditions were identical based on fitting BTCs of both tracers. We will therefore limit our discussion to $^3\text{H}_2\text{O}$ BTCs in the Results and Discussion section of this chapter.

Criteria for Distinguishing Equilibrium vs Nonequilibrium Transport

Equilibrium transport conditions were assumed when (i) the goodness of fit (r^2) using the PNE model did not result in improved r^2 values compared to the LEA model and (ii)

the optimized nonequilibrium parameters β and ω were 1 or ≥ 100 , respectively. When these criteria were met, optimized values of P and R_f were identical for both the PNE and LEA models. Conversely, PNE conditions were assumed, when higher r^2 values were obtained with the PNE model, and when $\beta < 1$ and $\omega < 100$.

Soil Water Characteristic and Pore Size Distribution

The procedure for obtaining $\theta(h)$ data (soil water characteristics) during soil column wetting and drying cycles was described in Chapter 2 (p. 12). Volumetric water contents obtained at h values between 0 and -70 cm were used to fit a parametric $\theta(h)$ model (van Genuchten, 1980):

$$\frac{\theta(h) - \theta_r}{\theta_s - \theta_r} = [1 + (\alpha|h|)^n]^{-m} \quad [16]$$

where θ_s represents the soil-water content measured at saturation ($\text{m}^3 \text{m}^{-3}$), θ_r is residual water content ($\text{m}^3 \text{m}^{-3}$, fitted), and α , n and m are fitting parameters describing the shape of the $\theta(h)$ relationship. The pore size distribution was estimated by relating the drained porosity [$\theta_s - \theta(h)$] to the minimum drained pore radius r as a function of h . Values of $r(h)$ may be obtained from the capillary equation (Jury et al., 1991):

$$r = -\frac{2\sigma \cos\gamma}{\rho_w g h} \quad [17]$$

where σ is the surface tension of water (0.073 N m^{-1} at 23°C), γ is the contact angle

between soil water and solids (assumed $\gamma = 0^\circ$), ρ_w is the density of water (10^3 kg m^{-3}), and g is the gravitational constant (9.8 m s^{-2}). The drained porosity at any h should consist of soil pores having radii larger than r .

RESULTS AND DISCUSSION

Effects of Matric Potential

An example series of $^3\text{H}_2\text{O}$ breakthrough curves (BTCs) as a function of h acquired with a single soil column is shown in Figure 5A-D. Each plot contains fitted BTCs obtained with the equilibrium (LEA) and nonequilibrium (PNE) models, and soil matric potentials measured at two column locations. At $h = -11 \text{ cm}$ (Fig. 5A), the $^3\text{H}_2\text{O}$ BTC is reasonably symmetrical and typical of equilibrium conditions. This observation was confirmed by the fact that (i) optimized Peclet numbers (P) and retardation factors (R_f) from the PNE and LEA models were identical, and (ii) β and ω of the PNE model were 1 and 100, respectively (Table 1). The optimized value $R_f = 1.22$ was used in model fits to the BTCs obtained at higher h .

Physical nonequilibrium conditions were evident in the $^3\text{H}_2\text{O}$ BTCs collected at $h = -5$ (PN11_4) and -3 cm (PN11_3). These BTCs occur earlier than at $h = -11 \text{ cm}$, and exhibit a more rapid increase in C/C_0 . Further, the PNE model fit the observed BTCs better than the LEA model (r^2 increased from 0.94 to 0.99 for PN11_4 and from 0.95 to 0.98 for PN11_3, Table 1), resulting in optimized values for the fraction of mobile water (β) of 0.44 (PN11_4) and 0.43 (PN11_3). The $^3\text{H}_2\text{O}$ BTC obtained under ponded conditions

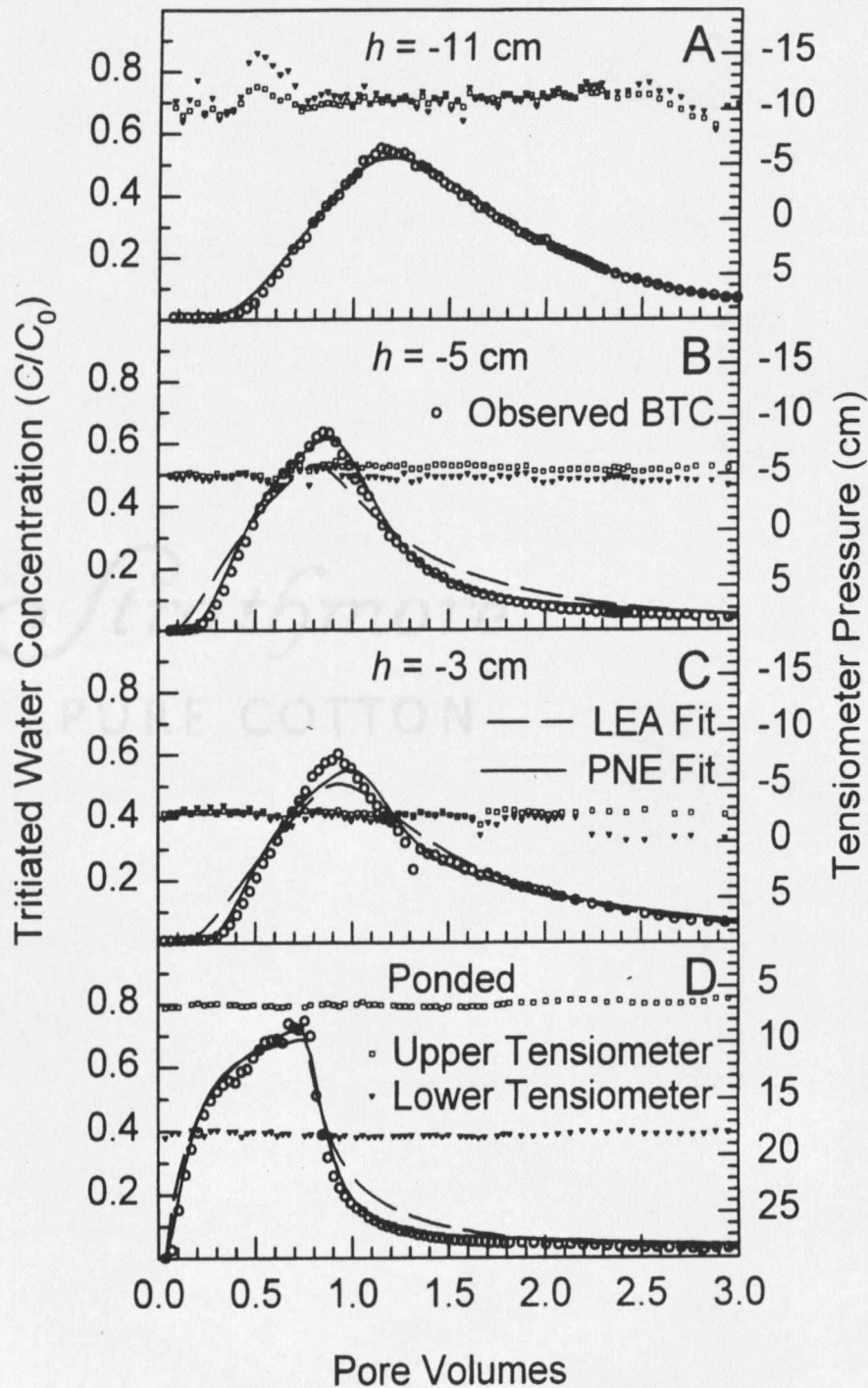


Figure 5. Example series of observed and fitted (LEA and PNE models) BTCs collected with soil column PN11 at various values of h . Each plot contains two series of soil matrix potentials measured at the two tensiometer locations. Note the positive pressures at both tensiometer positions in D, which were caused by low hydraulic conductivity of the bottom porous plate.

Table 1. Experimental conditions of the transport experiments using four undisturbed soil cores, and optimized model parameters from fitting $^3\text{H}_2\text{O}$ BTCs to solute transport models based on local equilibrium (LEA) and physical nonequilibrium (PNE) models.

Experiment ID†	Matric potential (h)	Soil water content (θ)	Relative saturation (θ/θ_s)	Pore water velocity (v)	Column length (L)	Pulse width	Fitting parameters							
							LEA model			PNE model				
	cm	$\text{m}^3 \text{m}^{-3}$		cm h^{-1}	cm	p. vol.	R_f †	P	r^2	R_f	P	β	ω	r^2
Column PN14														
PN14_3	-10	0.374	0.96	0.91	26.3	0.57	*1.18	6.2	0.995	*1.18	6.2	1	100	0.995
PN14_4	-24	0.367	0.94	0.20	26.3	0.65	1.18	17.6	0.993	1.18	17.5	1	100	0.993
Column PN13														
PN13_5	-3	0.360	0.98	0.96	25.9	0.79	*1.40	2.9	0.962	*1.38	4.2	0.51	3.8	0.984
PN13_4	-5	0.350	0.96	1.24	25.9	0.72	1.40	8.5	0.997	1.38	12.4	0.74	2.3	0.998
Column PN12														
PN12_2	ponded	0.394	1.00	2.64	25.8	0.68	*1.21	0.27	0.971	*1.21	2.0	0.29	0.21	0.999
PN12_4	-2	0.386	0.98	1.14	25.8	0.77	*1.21	5.53	0.951	*1.21	10.8	4E-4	13.0	0.992
PN12_5	-10	0.375	0.95	1.06	25.8	0.80	1.21	11.2	0.994	1.21	11.2	1	4E+5	0.994
Column PN11														
PN11_1	ponded	0.368	1.00	1.00	27.0	0.72	*1.24	0.24	0.967	*1.24	2.8	0.20	0.52	0.991
PN11_3	-3	0.369	1.00	0.78	27.0	0.73	*1.24	2.2	0.955	*1.24	19.9	0.43	1.04	0.979
PN11_4	-5	0.367	1.00	0.73	27.0	0.70	*1.24	1.3	0.942	*1.24	8.3	0.44	0.54	0.991
PN11_2	-11	0.363	0.99	0.35	27.0	0.75	1.24	5.3	0.996	1.24	5.3	1	100	0.996

† Asterisks indicate fixed values in fitting procedure.

‡ Notation: P (Location: A. H. Post Experimental Farm), N (native grassland site), 11-14 (core number), 1-5 (experiment number).

exhibited significant asymmetry, an extreme shift to the left and tailing, all characteristic of PNE (Fig. 5D). As expected, the PNE model fit the observed BTC better than the LEA model, resulting in optimized values of β and ω of 0.20 and 0.52, respectively.

The set of $^3\text{H}_2\text{O}$ BTCs obtained with column PN11 suggested that the transition from equilibrium to nonequilibrium transport conditions occurred between h of -5 and -11 cm. Experiments with additional undisturbed columns confirmed and narrowed the range of h values corresponding to the onset of PNE. All experiments performed at h of -5 cm (PN11_4 and PN13_4) or higher exhibited PNE, while experiments at h of -10 cm (PN14_3 and PN12_5) and lower exhibited equilibrium transport conditions (Table 1). Similar to the results of Seyfried and Rao (1987), there was no evidence from our data of increases in PNE when h was further decreased to -24 cm. These findings differ from results reported by Biggar and Nielsen (1960) and several other researchers (cf. references in Brusseau and Rao, 1990) who observed an increase in transport nonideality with decreasing values of h in homogeneous porous media. Apparently, the pore network in the soils used by Seyfried and Rao (1987) and in the current study were sufficiently interconnected that drainage of large pores did not result in the isolation of immobile water regions. The pore systems of homogeneously packed sand or soil columns may be more susceptible to forming immobile regions with decreasing water content (Brusseau and Rao, 1990).

Effects of Soil Properties

It must be stressed that physical nonequilibrium (PNE) does not depend directly on h , but h controls whether soil pores contain water, and hence potentially contribute to preferential flow. The presence of macropores in the soil is therefore essential for PNE to occur. Several studies have qualitatively found that with decreasing macroporosity (e.g., due to traffic, cropping system or tillage practice) the potential for PNE decreases (Li and Ghodrati, 1995; Singh and Kanwar, 1991; Wu et al., 1995; Munyankusi et al., 1994). Hypothetically, if the fraction of soil volume occupied by macropores was known, quantitative inferences about the potential extent of preferential flow events would be possible. The capillary equation (Eq. [17]) can be used to relate values of h corresponding to preferential flow to specific pore radii.

For undisturbed cores used in the current study, a transition from equilibrium to nonequilibrium transport conditions was observed at values of h between -5 and -10 cm. These matric potentials correspond to minimum drained pore radii of 300 and 150 μm , respectively. Because only one soil was tested, the current study was not suited for determining if these radii are representative for a wide variety of soils. In the following section, we show how our experimental design was used to determine pore size distributions in test columns. However, similar studies using a variety of soils would be necessary to verify the results and to correlate pore size distributions with the probability of PNE.

Paired measurements of θ and h were obtained during both wetting and drying cycles of columns PN14, PN13 and PN12, in hopes of determining the pore size fraction

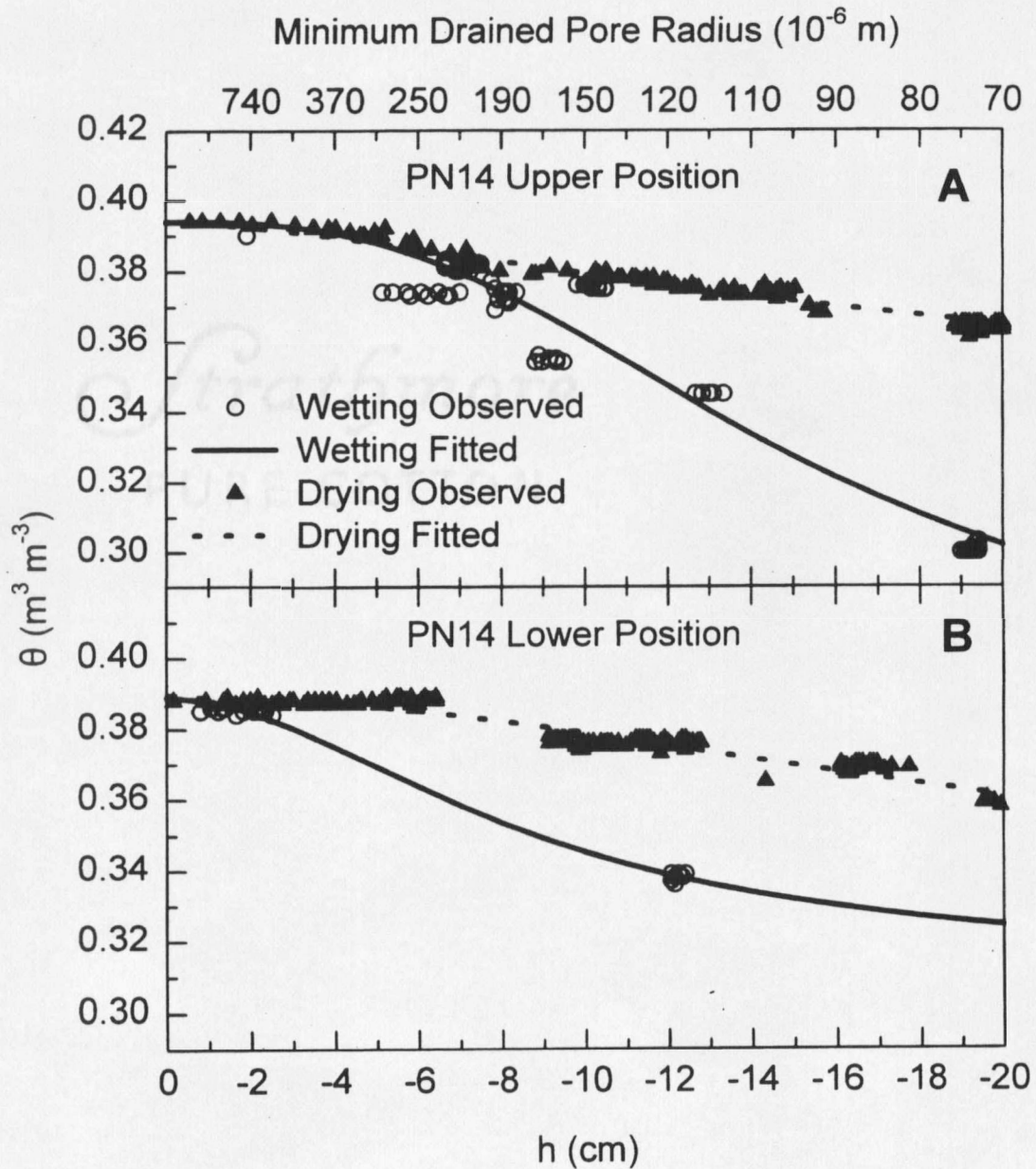


Figure 6. Water characteristic relationships [$\theta(h)$] for soil column PN14 generated at two depths (8 and 20 cm). Symbols represent measured $\theta(h)$ values, lines are least square fits to the van Genuchten (1980) model (optimized parameter values are shown in Table 2).

responsible for nonequilibrium solute transport. Figure 6 shows a typical example of the combined $\theta(h)$ relationships for wetting and drying (water characteristic) obtained at the two instrumented positions within column PN14. Establishing meaningful pore size distributions is complicated by the presence of considerable hysteresis between wetting and drying curves for both column positions, and by the variability in hysteresis observed between the two measurement locations within a column. For example, in column PN14, hysteresis was more pronounced at the upper than at the lower TDR waveguide-tensiometer position (6% vs 3% difference in θ , respectively, at $h = -20$ cm; Fig. 6A and B). Furthermore, some of the $\theta(h)$ curves exhibit no change in θ between $h = 0$ cm and -10 cm. For example, the water retention (or drying) curve at the lower position of column PN14 (Fig. 6B) shows a constant value of θ between $h = 0$ and -7 cm. This phenomenon is typically explained for *retention curves* by invoking an air entry pressure necessary for any initial displacement of pore water with air. However, another column (PN13, upper instrumented position) exhibited no significant change in θ between $h = 0$ and -10 cm for *both wetting and drying curves* (Fig. 7A and B).

The water characteristic data were fit to van Genuchten's model (van Genuchten, 1980; Eq. [16]) using nonlinear least squares optimization (Fig. 7, Table 2). Optimized parameters were obtained based on measured $\theta(h)$ pairs in the range $h = 0$ to -70 cm, which represents only the very wet portion of commonly studied $\theta(h)$ relationships [commonly, $\theta(h)$ values at dryer conditions include field capacity ($h \approx -3$ m) and permanent wilting point (-150 m)]. Inferences about the $\theta(h)$ relationship for the Amsterdam soil in the dryer range based on the optimized parameters using only the wet

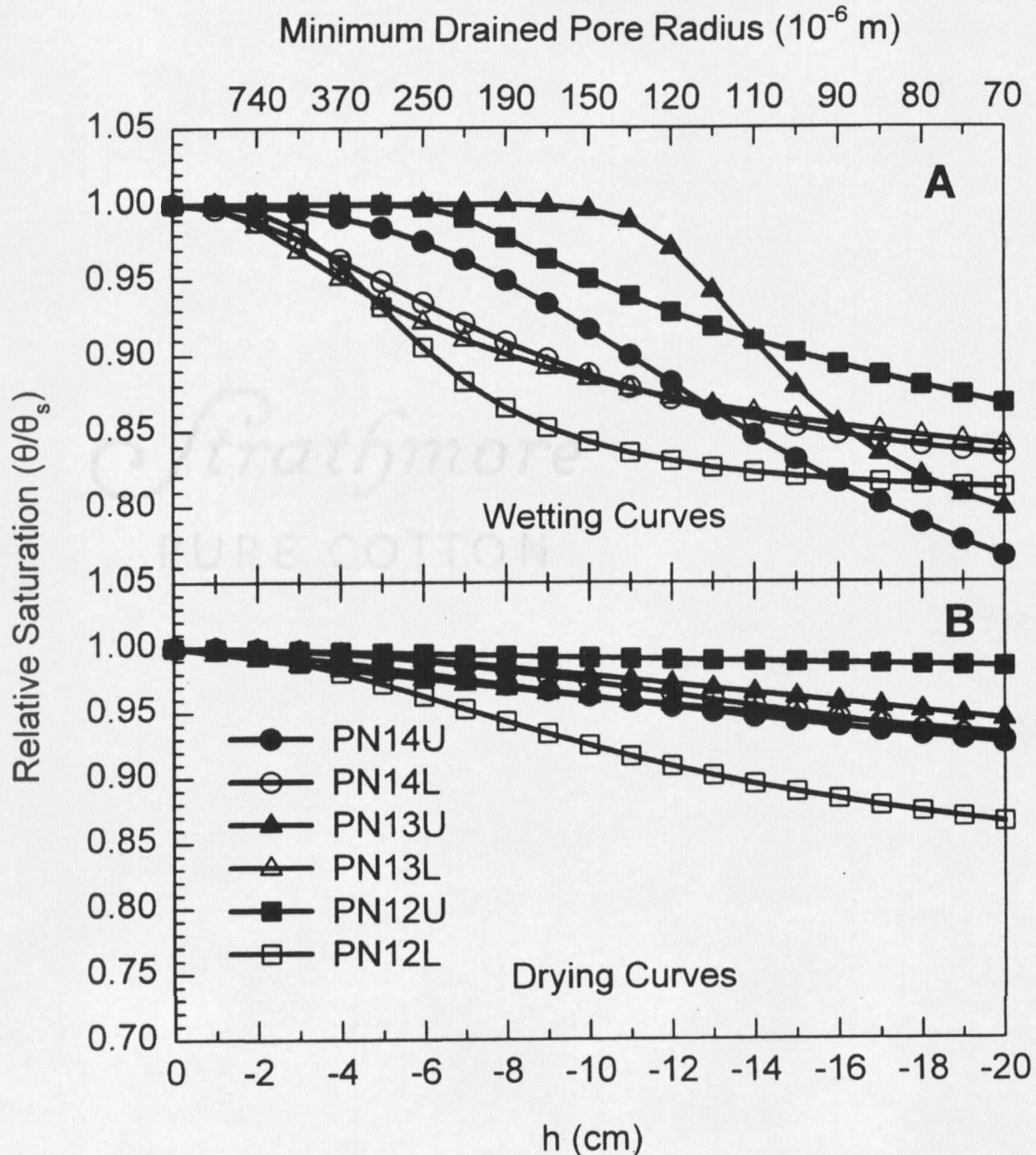


Figure 7. Fitted wetting (A) and drying curves (B) for both upper (closed symbols) and lower (open symbols) instrumented positions (indicated in legend by U or L, respectively). Optimized parameters (Table 2) were obtained by fitting van Genuchten's (1980, Eq. [16]) model to measured $\theta(h)$ data between $h = 0$ and -70 cm.

Table 2. Optimized parameters from fitting van Genuchten's (1980) model to $\theta(h)$ data collected during wetting and drying cycles of selected soil columns.

Instrumented Position	Cycle	θ_s (measured)	Fitting parameters				r^2
			θ_r	α	n	m	
		$m^3 m^{-3}$	$m^3 m^{-3}$				
Column PN14							
upper	wetting	0.394	0.26	0.07	2.77	1.00	0.94
	drying	0.394	0.33	0.05	1.51	1.00	0.98
lower	wetting	0.389	0.31	0.11	1.91	1.00	1.00
	drying	0.389	0.33	0.05	2.06	1.00	0.98
Column PN13							
upper	wetting	0.357	0.27	0.08	13.14	0.27	0.97
	drying	0.354	0.28	0.03	1.71	1.00	0.98
lower	wetting	0.384	0.26	0.36	2.70	0.12	0.94
	drying	0.383	0.27	0.01	1.00	1.00	1.00
Column PN12							
upper	wetting	0.402	0.00	0.15	12.92	0.01	0.96
	drying	0.386	0.00	0.00	1.00	0.33	0.85
lower	wetting	0.396	0.32	0.19	3.58	0.66	0.92
	drying	0.395	0.32	0.08	1.92	1.00	0.95

range are therefore not reliable. General features of the combined drying and wetting curves are as expected with more gradual slopes near saturation ($h = 0$ to approximately -5 cm), and a steeper portion at lower values of h (approximately -5 to -30 cm). At matric potentials below approximately -30 cm, the slopes become more gradual again and asymptotically approach the residual water content (θ_r). Figure 7 illustrates the wide range in $\theta(h)$ at values of $h > -20$ cm obtained from three undisturbed soil cores.

The optimized model parameters from the van Genuchten Equation (van Genuchten,

1980; Table 2) were used to estimate drained porosities $[\theta_s - \theta(h)]$ as a function of h and the corresponding minimum drained pore radius r (Fig. 8). Using this approach, pore size distributions at each instrumented position can be determined from individual wetting or

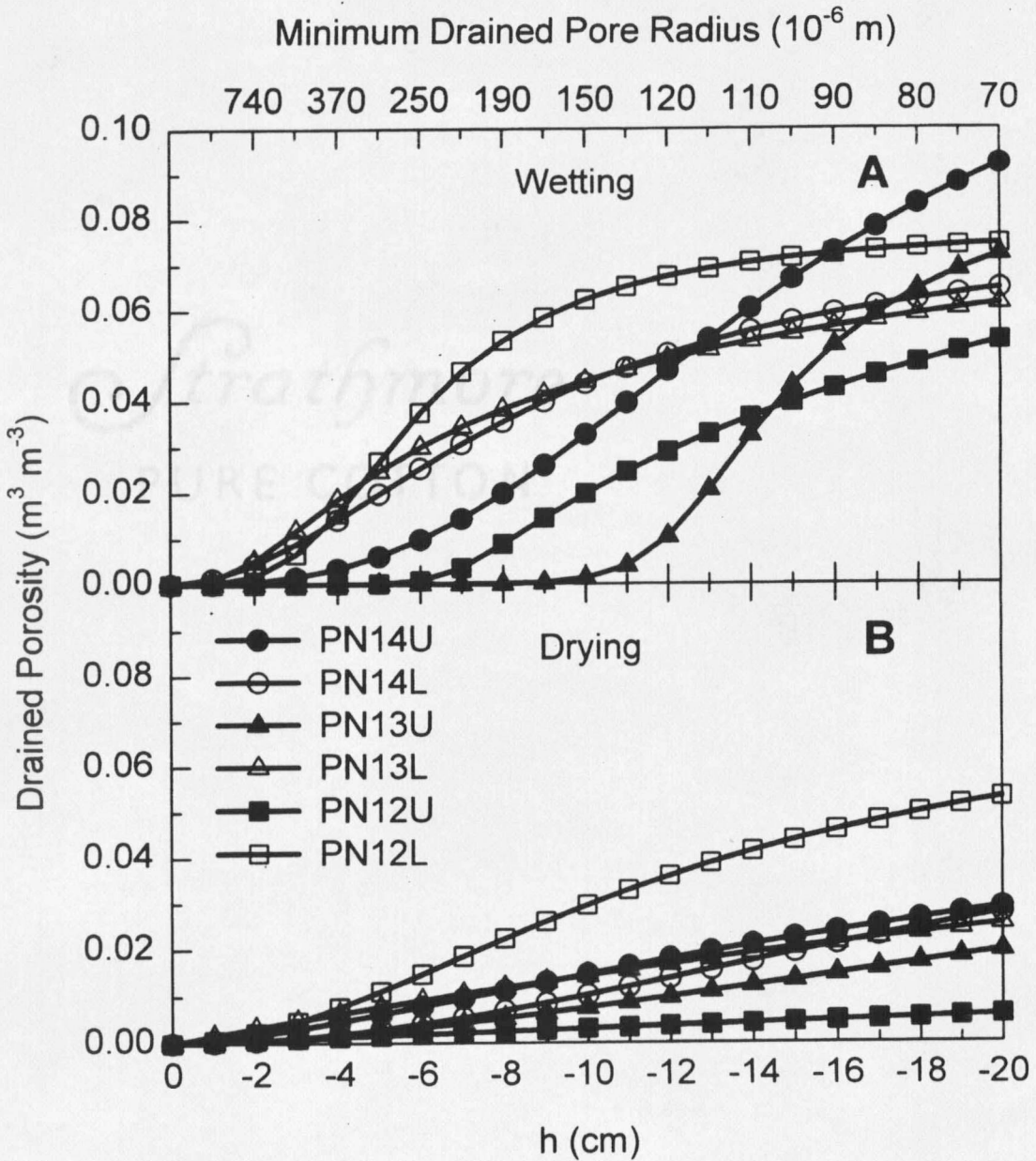


Figure 8. Estimated drained porosities $[\theta_s - \theta(h)]$ derived from the $\theta(h)$ curves shown in Fig. 7. Minimum drained pore radii (r) were calculated as a function of h using Eq. [17].

drying curves. The fractional soil volume corresponding to a range in pore radii can be obtained by the difference between drained porosities across the range of pore radii. Results of fractional soil volumes corresponding to a constant range in pore radii vary widely between and within columns, and do not allow for more than general conclusions. For example, the soil volume fractions represented by pores draining at $h = -10$ cm (radii of $150 \mu\text{m}$ and larger) range between 0.2% (PN13U) and over 6% (PN12L) of the soil volume as determined from the various wetting curves. For drying curves, soil volumes between 0.3% (PN12U) and 3% (PN12L) correspond to the same pore size fraction (i.e., $r > 150 \mu\text{m}$). Since all undisturbed soil cores were collected within 10 m from a consistent landscape position, the observed variation is most likely due to small-scale heterogeneities in θ within the soil columns. The TDR waveguides sample a limited soil volume weighted toward the paired rods (Knight, 1992). Small changes in h which cause a few large macropores to drain or fill may or may not correspond to changes in measured θ , depending on the position of the TDR waveguide relative to the affected pores. Gravimetric measurements may have yielded more representative results of average column θ .

In summary, preferential flow in several intact soil cores was consistently observed at values of h between 0 and approximately -10 cm. Based on the capillary equation, values of $h > -10$ cm correspond to pore sizes $>150 \mu\text{m}$. However, wide variations in pore size distributions and fractional drained porosities determined over this range in h do not support definitive conclusions concerning the fractional soil volume which contributes to preferential flow. Specifically, the drained porosities between $h = 0$ and -10 cm ranged from 0 and 6% of the total soil volume depending on which $\theta(h)$ curve is used to obtain

pore size distribution (Fig. 8). Our results represent an additional example of the difficulties in accurately defining the $\theta(h)$ relationship at the wet range, which would be necessary to assign specific fractions of soil volume responsible for the occurrence of nonequilibrium transport (Beven and Germann, 1982; Luxmoore et al., 1990). The authors believe, however, that the experimental apparatus employed in the current study could potentially generate pore size distribution data that are much more reproducible. In particular, the method of determining θ would have to be modified such that the measurements were representative of a large soil volume (ideally, the *representative elementary volume*; Hubbert, 1956; Bear, 1972). This could be accomplished by modifying the dimensions or number of TDR waveguides or by using gravimetric measurements.

Pore Water Velocity and Matric Potential

Pore water velocities (v) observed during the transport experiments decreased with decreasing matric potential (h). This was expected because of the reduction in the largest water-transmitting pores with decreasing h . However, observed decreases in v associated with the transition from saturated to unsaturated conditions were lower than those reported by other authors. Data presented in Germann and Beven (1981) show a difference of about two orders of magnitude between the hydraulic conductivity at saturation and at $h = -10$ cm. Seyfried and Rao (1987) observed an approximately twenty-fold decrease in v when h was reduced from 0 to -10 cm and more than a 100 fold decrease in v when h was reduced from 0 to -20 cm. In the current study, changes in v (corresponding to changes in h) did not exceed one order of magnitude (Table 1), which was due in part

to flow restrictions through the porous plate under saturated (ponded) conditions. Positive pressures observed within our columns during saturated transport experiments indicated that pore water velocities at saturation were constrained by the hydraulic conductivity of the porous plate rather than the saturated hydraulic conductivity of the soil. Although this was also true for the saturated experiments performed by Seyfried and Rao (1987), their bottom column boundary (fritted glass plate) supported a higher flow rate than the stainless steel plates used in this study. There were no indications in the current study that the bottom porous plates caused restrictions in water flow at values of $h < 0$.

Another reason for the relatively minor decrease in v with decreasing h observed in the current study may be due to the relatively small number of soil macropores which drained within $h = 0$ and $h = -10$ cm. Specifically, Seyfried and Rao (1987) reported a decrease in θ of $0.04 \text{ m}^3 \text{ m}^{-3}$ (0.57 to 0.53) when h was reduced from 0 to -10, compared to reductions in θ of $< 0.02 \text{ m}^3 \text{ m}^{-3}$ in the current study over the same range in h . This suggests the presence of a considerably higher number of soil pores with radii $> 150 \mu\text{m}$ (drained at $h = -10$ cm) in Seyfried and Rao's (1987) soil than in the soil used in this study.

Pore Water Velocity and Physical Nonequilibrium

Within each individual column tested, the onset of PNE conditions associated with greater h was also associated with increases in pore water velocity (v , Table 1). Consequently, effects of h on PNE were confounded with possible effects of changing v . A series of experiments with relatively uniform v ($\approx 1 \text{ cm h}^{-1}$) was selected from replicate

columns where increases in h exhibited the same effects on PNE as discussed for each individual column (Fig. 9). Optimized values for β and ω are 1 and 100, respectively, for the experiment at $h = -10$ cm (PN12_5, Fig. 9A) indicating equilibrium transport conditions. For other experiments at $h \geq -5$ cm, optimized values for β and ω are <1 and <100 , respectively, suggesting that PNE was important. The changes in relative saturation (θ/θ_s , Fig. 9) indicate that with increasing h , pores with increasing radii contribute to the water transport. The relative uniformity of v in the unsaturated columns ($h < 0$) can therefore only be explained in terms of differences in (water conducting) pore size distribution, although results from $\theta(h)$ curves under wetting and drying conditions were not sensitive enough to reveal these (cf. p. 34-41).

Inferences concerning the likelihood of nonequilibrium transport under field conditions can be made using information on (i) pore water velocities necessary for occurrence of PNE, and (ii) expected pore water velocities as a result of rainfall or irrigation events. PNE was observed in our soil columns at pore water velocities ranging from 0.73 to 2.64 cm h^{-1} . The lowest v used in our experiments which resulted in preferential flow was 0.73 cm h^{-1} (PN11_4). This v corresponds to a water flux density (Darcy velocity) of 0.27 cm h^{-1} , which is often exceeded for this soil during moderate rain events, irrigation, and during snowmelt. Of course, this can only be a rough estimation; calculating actual probabilities of preferential flow events from our experimental data is difficult, since tracer transport experiments were performed under steady state conditions and did not consider effects of the initial soil water content (Shipitalo and Edwards, 1996). Also, lateral surface water flow, even in moderate amounts, may influence locally observed

